Integrated Observer-Based Terminal Sliding-Mode Speed Controller for PMSM Drives Considering Multisource Disturbances

Minghe Tian, Tianqing Wang, Yong Yu, Qinghua Dong, Bo Wang, *Member, IEEE*, and Dianguo Xu, *Fellow, IEEE*

***Abstract*—There are multisource disturbances in permanent magnet synchronous motor (PMSM) drives, which can lead to speed fluctuations, deteriorating the speed control performance. The existing terminal sliding mode controller (TSMC) methods cannot achieve the desired control performance when they are applied as the speed controller. This is because these methods do not overcome the inherent problems of the traditional TSMC, such as the chattering phenomenon and differential calculation. To solve this problem, this article proposes an integrated observer-based TSMC for the speed regulation of PMSM drives. First, a TSMC is proposed. Then, an error-based extended state observer with generalized integrators is proposed and it is introduced to the proposed TSMC. In the proposed scheme, the proposed observer is employed to estimate the multisource disturbances, which are adapted to the TSMC to attenuate the chattering level. In addition, the proposed observer contains the speed error differential signal, which can be employed for the calculation of the TSMC. Thus, the proposed scheme can solve the inherent problems of traditional TSMC. Compared with the existing TSMC methods, the proposed scheme can achieve the desired control performance even in the presence of multisource disturbances when it is employed as the speed controller. Finally, the effectiveness of the proposed scheme is validated on a 2.2-kW PMSM platform.**

***Index Terms*—Error-based extended state observer, generalized integrator, permanent magnet synchronous motor (PMSM), speed loop, terminal sliding mode controller.**

Nomenclature

PMSM	Permanent magnet synchronous motor.
PI controller	Proportional-integral controller.
SMC	Sliding mode controller.
TSMC	Terminal sliding mode controller.
EESO	Error-based extended state observer.
GI	Generalized integrator.

Manuscript received 12 December 2023; revised 24 February 2024; accepted 30 March 2024. Date of publication 4 April 2024; date of current version 16 May 2024. Recommended for publication by Associate Editor B. Singh. *(Corresponding author: Yong Yu.)*

The authors are with the School of Electrical Engineering and Automation, Harbin Institute of Technology, Harbin 150001, China (e-mail: tian_mh@stu.hit.edu.cn; 19S006067@stu.hit.edu.cn; yuyong@hit.edu.cn; dqh@stu.hit.edu.cn; wangbohit@hit.edu.cn; xudiang@hit.edu.cn).

Color versions of one or more figures in this article are available at https://doi.org/10.1109/TPEL.2024.3384991.

Digital Object Identifier 10.1109/TPEL.2024.3384991

I. Introduction

THE speed control quality of permanent magnet synchronous motor (PMSM) has been put forward high requirements by many high-performance applications, especially in high-precision computerized numerical control machine tools, laser cutting systems, and robotic systems [1], [2]. However, the speed quality is deteriorated by multisource disturbances [3], which can limit the application of PMSMs in advanced manufacturing industries. Based on the effects of the multisource disturbances, they can be divided into periodic and aperiodic disturbances [4], [5], as shown in Table I. In Table I, n is a positive integer, ω_e is the electrical angular speed, and N_c is the least common multiple between the number of slots and pole pairs. These aperiodic and periodic disturbances can lead to serious aperiodic and periodic speed fluctuations, which are intolerable for high-precision industrial applications. Therefore, it is necessary to study the multisource disturbance suppression strategy for the speed loop to improve the speed control quality.

To suppress the multisource disturbances in the speed loop, many control strategies have been studied, such as two degree-of-freedom PI controller, adaptive controller, fuzzy controller, active disturbance rejection controller, and sliding mode controller (SMC) [6], [7], [8], [9]. In these strategies, the SMC is regarded as an effective strategy for its distinguished features, such as easy implementation and strong robustness to parameter uncertainties and external disturbances [10], [11], [12]. Based on this, the SMC has been widely applied in PMSM drives. However, the robustness of SMC can only be guaranteed by the selection of large control gains, while the large gains can cause the undesired chattering phenomenon, which can excite high-frequency dynamics [13]. In addition, since the traditional SMC employs a linear sliding surface, its convergence rate can only at best be exponential with an infinite settling time. To solve the problems, different improved SMC methods have been proposed [14], [15], [16], such as observer- based SMC, terminal sliding mode controller (TSMC), and observer-based TSMC. Table II shows the advantages and disadvantages of the existing improved SMC methods. Then, the improved SMC methods listed in Table II are explained sequentially.

First, to reduce the chattering level of the traditional SMC, the observer-based SMC method is proposed [17], [18]. This method is to estimate the disturbances using an observer, then

TABLE I
MULTISOURCE DISTURBANCES IN PMSM DRIVES [3]

Disturbance classification	Disturbance type	Symbol	Frequency
Aperiodic disturbance	Load torque mutation	T_l	/
	Friction torque	T_f	/
	Parameter mismatch	T_p	/
Periodic disturbance	Flux harmonic	ψ_h	$6n\omega_e$
	Voltage harmonic	u_h	$6n\omega_e$
	Torque harmonic caused by current sampling error	T_i	$\omega_e / 2\omega_e$
	Cogging torque	T_{cog}	$nN_c\omega_e$

compensate for them. After compensation for these disturbances, it is pointed out that the switching gain of SMC can be selected smaller to reduce chattering. For instance, in [18], a chattering attenuation disturbance observer is used to achieve chattering reduction in the SMC. The proposed observer with SMC is employed in PMSM drives to improve the control performance. However, since the observer-based SMC still uses a linear sliding surface, its convergence rate is slow.

To improve the dynamic response performance, a direct way is to introduce nonlinear sliding surfaces. Based on this, the TSMC is studied [19], [20], [21]. The TSMC has a nonlinear sliding surface, which can ensure the finite-time convergence of states during the sliding mode stage. However, like the traditional SMC, the robustness of TSMC can only be guaranteed by the selection of large control gains, while the large gains can lead to the undesired chattering phenomenon.

Compared with the observer-based SMC and pure TSMC, the observer-based TSMC is regarded as an effective strategy. This method not only uses an observer to suppress disturbances to reduce the chattering level, but also uses a nonlinear sliding mode surface to improve the convergence rate. Based on this, this method has been widely used in PMSM drives [22], [23], [24]. In [25], for instance, a disturbance observer is applied to enhance the robustness of the TSMC. The proposed method in [25] is employed as the speed controller to improve the speed control accuracy. Despite having an excellent control impact, as indicated in Table II, this method still has three issues that require further study.

1) The existing methods do not consider the impact of periodic disturbances.
2) The existing methods contain the error differential signal. However, the differential calculation is likely to amplify the measurement noise in the system, which is not tolerated by the practical system [26].
3) The existing methods are relatively complex and have a dispersed structure, which is in two-degree-of-freedom form. However, most industrial controllers are implemented as single blocks in one-degree-of-freedom error-driven form [27]. Thus, the existing methods are not directly compatible with industrial controllers.

Recently, an error-based extended state observer (EESO) has been proposed. Unlike the traditional observers, whose input is system output [28], [29], the input of the EESO is the system error signal [30]. This indicates that the EESO is designed based on the error-dynamic equation. The EESO can accurately estimate the aperiodic disturbance. However, it cannot fully estimate the periodic disturbance due to the limited control bandwidth. Thus, the pure EESO cannot accurately estimate the multisource disturbances in the speed loop. To address the problem, a GI-EESO is proposed in this article. In the proposed observer, the GI can expand the bandwidth of the EESO at a specific frequency [8], [31], thereby further observing the corresponding periodic disturbance.

In the article, an integrated observer-based TSMC is proposed for the speed loop of PMSM drives. The proposed GI-EESO is introduced to estimate the multisource disturbances in the speed loop, which are adapted to the TSMC to avoid chattering phenomena. The contributions of this article can be summarized into the following three aspects.

1) Compared with the existing observer-based TSMC, the proposed scheme further considers the periodic disturbances.
2) The proposed GI-EESO contains the error differential signal, which can be employed for the calculation of the TSMC. Thus, the proposed scheme can avoid the differential calculation.
3) Both the proposed GI-EESO and the TSMC are designed based on the same error dynamic equation of the speed loop. Thus, the GI-EESO and the TMSC can enable integrated design, and the proposed scheme is an integrated observer-based TSMC structure. In addition, the input of the GI-EESO is the same as the TSMC, which is the error between the reference speed and the feedback speed. This indicates the proposed scheme is an error-driven form. Thus, it is well compatible with industrial controllers.

The rest of this article is organized as follows. In Section II, the speed loop control objective is described. In Section III, a TSMC is designed and analyzed. In Section IV, an integrated observer-based TSMC is proposed for the speed loop of PMSM drives. The experiments are conducted on a 2.2-kW PMSM setup to show the validity of the proposed scheme in Section V. Finally, Section VI concludes this article.

II. SPEED LOOP CONTROL OBJECTIVE

A. Mechanical Dynamics With Multisource Disturbances

The mechanical dynamics of the PMSM can be written as [5]

$$\frac{d}{dt}\omega_m = \frac{1}{J}T_e - \frac{1}{J}T_l - \frac{1}{J}B\omega_m \tag{1}$$

where ω_m is the mechanical angular velocity, J is the rotational inertia, T_l is the load torque, B is the viscous friction coefficient, and T_e is the electromagnetic torque, which can be written as

$$T_e = \frac{3}{2}p_n\psi_f I_s \sin\beta + \frac{3}{2}p_n\left(L_d - L_q\right)I_s^2 \sin\beta\cos\beta \tag{2}$$

where p_n is the number of pole pairs, ψ_f is the flux linkage, I_s is the stator current, β is the electrical angle between the stator flux linkage and the permanent magnet flux linkage, and L_d and L_q are the d- and q-axis inductances, respectively.

TABLE II
ADVANTAGES AND DISADVANTAGES OF THE EXISTING IMPROVED SMC METHODS

Method	Chattering level	Convergence rate	Periodic disturbance suppression	Error differential information	Structure
Traditional SMC [13]	high	slow	not considered	necessary	one-degree-of-freedom form
Existing observer-based SMC [17], [18]	low	slow	not considered	necessary	two-degree-of-freedom form
TSMC [19]-[21]	high	fast	not considered	necessary	one-degree-of-freedom form
Existing observer-based TSMC [22]-[25]	low	fast	not considered	necessary	two-degree-of-freedom form

Substituting (2) into (1) can yield

$$\frac{d}{dt}\omega_m = bI_s + \frac{1}{J}T_r - \frac{1}{J}T_l - \frac{1}{J}B\omega_m, \quad b = \frac{3}{2J}p_n\psi_f \sin\beta \tag{3}$$

where $T_r = \frac{3}{2}p_n(L_d - L_q)I_s^2 \sin\beta\cos\beta$.

Considering the periodic disturbances, such as flux harmonic, cogging torque, torque harmonic caused by current sampling error, and others [3], [4], [5], the PMSM mechanical dynamics can be rewritten as

$$\frac{d}{dt}\omega_m = bI_s + \frac{1}{J}T_r - \frac{1}{J}T_l - \frac{1}{J}B\omega_m + \frac{1}{J}T_{har} \tag{4}$$

where $T_{har} = g(\psi_h, u_h, T_{cog}, T_i)$. Here, T_{har} is defined as the total torque harmonic in the speed loop, ψ_h is the flux harmonic, u_h is the voltage harmonic, $T_{\rm cog}$ is the cogging torque, and T_i is the torque harmonic caused by current sampling error. Given that many papers have already modeled these periodic disturbances, we will not provide models for these periodic disturbances.

Define f_{ms} to denote the multisource disturbance, the PMSM mechanical dynamics can be further rewritten as

$$\frac{d}{dt}\omega_m = b_0 I_s + f_{ms} \tag{5}$$

where $f_{ms} = \Delta b I_s + \frac{1}{J}T_r - \frac{1}{J}T_l - \frac{1}{J}B\omega_m + \frac{1}{J}T_{har}$,$\Delta b = b - b_0$, and b_0 is the nominal value of the parameter b.

According to [8], the multisource disturbance f_{ms} satisfies the following practical supposition.

Supposition 1: It is differentiable, and its differential value is bounded.

B. Control Objective

According to (5), the control objective is to force the output speed to follow the reference speed by manipulating the current. However, there are multisource disturbances in the speed loop. They can inevitably cause serious speed fluctuations and destroy the speed steady-state performance. The objective of this article is to minimize the speed fluctuations in the presence of multisource disturbances. In addition, it should be noted that the reference speed (ω_{ref}) satisfies the following supposition.

Supposition 2: It is bounded and known at the current time instant t.

Supposition 3: Its consecutive first and second derivatives exist for all $t > 0$ and are bounded.

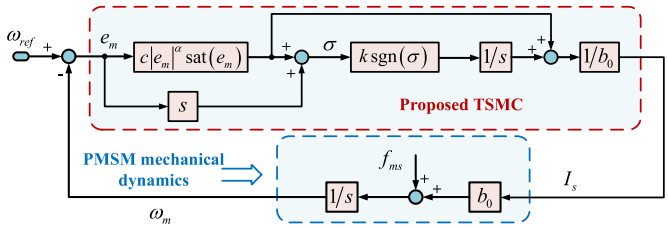

Fig. 1. Block diagram of the speed loop with the proposed TSMC.

From (5), if the tracking error is defined as $e_m = \omega_{ref} - \omega_m$, the tracking error dynamics can be derived as

$$\frac{d}{dt}e_m = f_e - b_0 I_s, \quad f_e = \frac{d}{dt}\omega_{ref} - f_{ms} \tag{6}$$

where f_e is the redefined multisource disturbance in the error-based form. According to the effects of these disturbances, multisource disturbances can be divided into periodic and aperiodic disturbances [4]. Thus, the multisource disturbances can be expressed as

$$f_e = f_p + f_{ap} \tag{7}$$

where $f_p = -\frac{1}{J}T_{har}$, $f_{ap} = \frac{d}{dt}\omega_{ref} - \Delta b I_s - \frac{1}{J}T_r + \frac{1}{J}T_l + \frac{1}{J}B\omega_m$, f_p is periodic disturbance, and f_{ap} is aperiodic disturbance.

Remark 1: According to (6), the control objective of the speed loop has been changed to keep the tracking error (e_m) at zero in the presence of multisource disturbances affecting the speed loop through the control input channel.

Remark 2: According to the suppositions 1–3, the new multisource disturbance is differentiable, and its differential value is bounded and defined by $f_e^* = \sup|df_e/dt|$.

III. TERMINAL SLIDING MODE CONTROLLER

In this section, a TSMC is first proposed for the speed loop of PMSM drives. Then, the stability of the proposed TSMC is analyzed in detail.

A. Design of the Proposed TSMC

Fig. 1 demonstrates the block diagram of the speed loop with the proposed TSMC. According to Fig. 1, the design of TSMC can be divided into two steps, as follows.

1) Design the Sliding Mode Surface of the Proposed TSMC: To guarantee fast and high-precision tracking performance, the following sliding mode surface is proposed:

$$\sigma = \frac{d}{dt}e_m + c|e_m|^{\alpha} sat\,(e_m)\,,$$

$$sat\,(e_m) = \begin{cases} 1, & e_m > \Delta e_m \\ e_m, & e_m \le |\Delta e_m| \\ -1, & e_m < -\Delta e_m \end{cases} \tag{8}$$

where $c > 0$, and $0 < \alpha < 1$.

When the closed-loop system is driven to reach the sliding mode $\sigma = 0$, the convergence trajectory of the system will be determined by the following nonlinear equation:

$$\frac{d}{dt}e_m + c|e_m|^{\alpha} sat\,(e_m) = 0. \tag{9}$$

From (9), the convergence time of the error can be solved as

$$t_c\,(e_m) = \begin{cases} \frac{1}{c(1-\alpha)}\left[|e_m(0)|^{1-\alpha} - |e_m|^{1-\alpha}\right] & |e_m| > |\Delta e_m| \\ \frac{1}{c\alpha}\left[|e_m|^{-\alpha} - |\Delta e_m|^{-\alpha}\right] & \\ +\frac{1}{c(1-\alpha)}\left[|e_m(0)|^{1-\alpha} - |\Delta e_m|^{1-\alpha}\right], & |e_m| < |\Delta e_m| \end{cases} \tag{10}$$

where $e_m(0)$ is the initial value of the speed error.

According to (10), the convergence time is related to two parameters, including c and α.

2) Design the Control Law of the Proposed TSMC: The control law of the proposed TSMC should be designed such that σ satisfies the following sliding mode condition:

$$\sigma\frac{d}{dt}\sigma < 0. \tag{11}$$

If condition (11) is satisfied, σ can approach zero in finite time. Based on (8) and (11), the control law of the proposed TSMC can be designed as follows:

$$\begin{cases} I_s = I_{eq} + I_n \\ I_{eq} = \frac{1}{b_0}c|e_m|^{\alpha} sat\,(e_m) \\ \frac{d}{dt}I_n = \frac{1}{b_0}k\mathrm{sgn}\,(\sigma) \end{cases} \tag{12}$$

where k is the control gain of the control law.

According to (12), it can be seen that the stator current I_s is calculated by two parts: 1) one is the equivalent control term I_{eq} and 2) the other is the SMC term I_n. The analysis of the two terms is presented as follows.

1) The first term (I_{eq}) is calculated based on the PMSM mechanical dynamics [seen (6)] and the sliding mode surface [seen (9)]. Neglecting the multisource disturbance f_e in (6), the ideal mechanical dynamics can be written as

$$\frac{d}{dt}e_m = -b_0 I_s. \tag{13}$$

Combining (9) and (13), the equivalent control term (I_{eq}) can be derived.

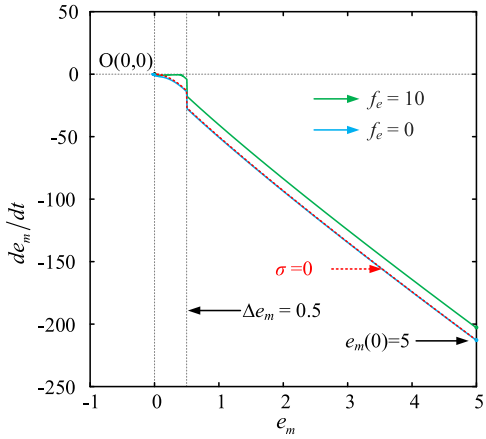

Fig. 2. Convergence trajectory of the proposed TSMC.

2) The second term (I_n) is mainly used to compensate for the multisource disturbance f_e to ensure that the system state variables can converge to the sliding mode surface. The reason is explained as follows.

Substituting the control law in (12) into the tracking error dynamics in (6) can obtain

$$\frac{d}{dt}e_m = f_e - c|e_m|^{\alpha} sat\,(e_m) - \int k\mathrm{sgn}\,(\sigma)\,dt. \tag{14}$$

According to (8), the (14) can be rewritten as

$$\sigma = \frac{d}{dt}e_m + c|e_m|^{\alpha} sat\,(e_m) = f_e - \int k\mathrm{sgn}\,(\sigma)\,dt. \tag{15}$$

From (14) and (15), there are two possible trajectories for error convergence. *1) The gain c is larger than the gain k.* In this case, the equivalent control term (I_{eq}) plays a much greater role than the disturbance compensation term (I_n) in the initial stage, and the convergence trajectory will converge along a direction similar to the sliding mode surface. As it approaches zero, the effect of I_{eq} decreases, and I_n begins to play the predominant role until the error converges to zero. *2) The gain k is larger than the gain c.* In this case, I_n plays a major role in the initial stage to quickly compensate for the total disturbance. Once the disturbance is fully compensated, it converges to the sliding mode surface ($\sigma = 0$). Then, I_{eq} plays a major role until the error converges to zero.

In this article, to reduce chattering level, a smaller switching gain k and a larger gain c are selected. Thus, the convergence trajectory follows the first case, as shown in Fig. 2. The tuning parameters are set as follows: $c = 50$, $\alpha = 0.9$, $k = 5$, $\Delta e_m = 0.5$, and $e_m(0) = 5$.

B. Stability Analysis of the Proposed TSMC

Substituting (6) into (8) can yield

$$\sigma = f_e - b_0 I_s + c|e_m|^{\alpha} sat\,(e_m)\,. \tag{16}$$

Substituting I_s in (12) into (16) can yield

$$\sigma = f_e - b_0 I_{eq} - b_0 I_n + c|e_m|^{\alpha} sat\,(e_m) = f_e - b_0 I_n. \tag{17}$$

According to (12) and (17), the derivative of the sliding mode surface can be derived as follows:

$$\frac{d}{dt}\sigma = \frac{d}{dt}f_e - b_0\frac{d}{dt}I_n = \frac{d}{dt}f_e - k\mathrm{sgn}(\sigma). \tag{18}$$

According to (18), the sliding mode condition (11) can be proven as follows:

$$\begin{aligned}\sigma\frac{d}{dt}\sigma &= \sigma\left[\frac{d}{dt}f_e - k\mathrm{sgn}(\sigma)\right] = -k|\sigma| + \sigma\frac{d}{dt}f_e \\ &\le -k|\sigma| + |\sigma|f_e^* = -(k - f_e^*)|\sigma|.\end{aligned} \tag{19}$$

According to (19), to satisfy the condition in (11), the control gain k should satisfy the following condition:

$$k > f_e^*. \tag{20}$$

Once the condition in (20) is satisfied, the speed error e_m can converge to zero in finite time.

IV. Proposed Integrated Observer-Based TSMC

Although the TSMC proposed in Section III can achieve good control effects, it still has some inherent problems of the SMC. Pure TSMC cannot achieve the desired control result when it is employed as the speed controller. The reasons can be summarized in the following two aspects.

1) To ensure that the proposed TSMC is robust to the multisource disturbance in the speed loop, a large switching gain (control gain k) is desired. However, this can lead to the undesired chattering problem.
2) The design of the proposed TSMC requires an available error differential signal [see (8)]. However, the differential calculation is likely to amplify the measurement noise in the system, which is not tolerated by the practical system [26].

To address the two problems, an integrated observer-based TSMC is proposed. In this section, the overall structure of the proposed scheme is first described. Then, the design process, stability analysis, and parameter selection rules of the proposed scheme are presented in sequence.

A. Structure Description of the Proposed Scheme

Fig. 3 illustrates the block diagram of the field-oriented control (FOC)-based PMSM drives with the proposed scheme. From Fig. 3, the PMSM control system adopts a cascade dual closed-loop structure, including the current loop and the speed loop. The current loop is controlled by the PI controllers, which generate the d- and q-axis reference voltages. The maximum torque per ampere (MTPA) algorithm is employed to calculate the d- and q-axis reference currents. The speed loop is controlled by the proposed scheme, which generates the stator current I_s. From Fig. 3, the proposed scheme contains two parts: 1) the first part is the GI-EESO and 2) the second part is the TSMC. In the GI-EESO, the integral term can estimate the aperiodic disturbances in the speed loop, such as load torque mutation. While the GIs can estimate the periodic disturbances, such as torque harmonic caused by current sampling error. Thus, the GI-EESO can estimate the multisource disturbance, which

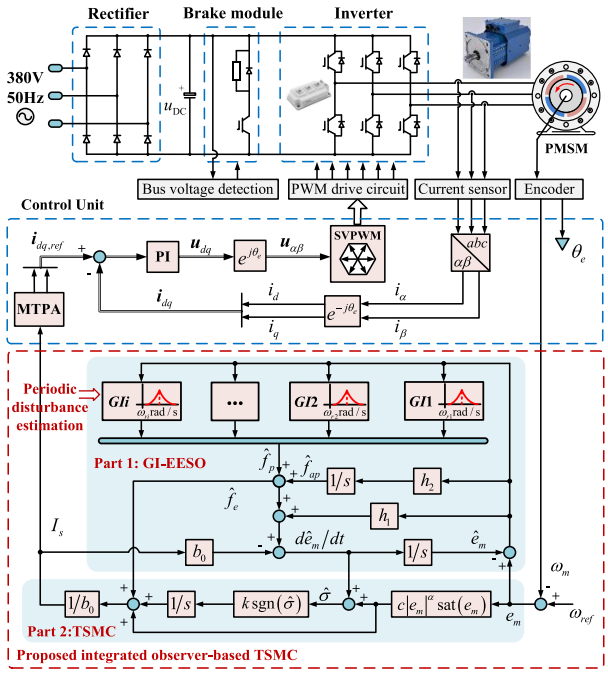

Fig. 3. Block diagram of the FOC-based PMSM drives with the studied scheme.

is adapted to the TSMC to enhance its robustness. This can help to select a smaller value for the switching gain (control gain k) of TSMC to reduce chattering level. Furthermore, from Fig. 3, the GI-EESO contains differential information of the speed error, which is employed to calculate the sliding mode surface of the TSMC. Therefore, the proposed scheme solves the inherent problems of pure TSMC. In addition, the input of the GI-EESO is the same as the TSMC, which is the error between the reference speed and the feedback speed. This indicates the proposed scheme is an error-driven form. Compared with the existing observer-based SMC schemes [22], [23], [24], [25], the structure of the proposed scheme is integrated. Therefore, it has benefits similar to those of the PI controller, such as compact structure and industry-proven form, and it is well compatible with industrial controllers.

According to Fig. 3, the design of the proposed scheme can be designed in the following two steps.

Step 1: Design the GI-EESO of the proposed scheme.

In the speed loop, compared to the speed harmonics caused by cogging torque, flux harmonics, and inverter nonlinearity, the speed harmonics caused by current sampling error are more serious [4]. There are first and second speed harmonics caused by the current sampling error in the experimental platform used in the lab. Therefore, two GIs are employed to optimize the EESO to estimate the corresponding speed harmonics in this article.

Taking the disturbance f_e as an extended state variable, the tracking error dynamics (6) can be further written in extended state equation form as follows:

$$\begin{cases}\frac{d}{dt}e_m = f_e - b_0 I_s \\ \frac{d}{dt}f_e = h_e\end{cases} \tag{21}$$

where h_e is the differential value of the disturbance f_e.

According to (21), the GI-EESO can be designed as follows:

$$\begin{cases} \frac{d}{dt}\hat{e}_m = \hat{f}_e - b_0 I_s + h_1\left(e_m - \hat{e}_m\right), \quad \hat{f}_e = \hat{f}_{ap} + \hat{f}_p \\ \frac{d}{dt}\hat{f}_{ap} = h_2\left(e_m - \hat{e}_m\right), \quad \hat{f}_p = z_2 + z_4 \\ \frac{d}{dt}z_1 = z_2 \\ \frac{d}{dt}z_2 = -\omega_{r1}^2 z_1 + k_{r1}\left(e_m - \hat{e}_m\right) \\ \frac{d}{dt}z_3 = z_4 \\ \frac{d}{dt}z_4 = -\omega_{r2}^2 z_3 + k_{r2}\left(e_m - \hat{e}_m\right) \end{cases} \tag{22}$$

where the symbol "^" denotes the estimated value, and h_1 and h_2 are the GI-EESO gains. z_1, z_2, z_3, and z_4 are the state variables of the two GIs. k_{r1} and k_{r2} are the gains. ω_{r1} and ω_{r2} are the angular frequencies of the periodic disturbances.

Supposition 4: The estimated error can exactly keep up with the actual speed error, this means $e_m - \hat{e}_m = 0$.

Step 2: Design the TSMC of the proposed scheme.

By replacing de_m/dt with $d\hat{e}_m/dt$ estimated by the GI- EESO, the sliding mode surface in (8) can be rewritten as

$$\hat{\sigma} = \frac{d}{dt}\hat{e}_m + c|e_m|^{\alpha} sat\left(e_m\right). \tag{23}$$

Based on (12), (22), and (23), the control law of the TSMC can be rewritten as

$$\begin{cases} I_s = I_{eq} + I_n + \frac{1}{b_0}\hat{f}_e \\ I_{eq} = \frac{1}{b_0} c|e_m|^{\alpha} sat\left(e_m\right) \\ \frac{d}{dt}I_n = \frac{1}{b_0} k \mathrm{sgn}\left(\hat{\sigma}\right). \end{cases} \tag{24}$$

From (23) and (24), compared with the TSMC proposed in Section III, the TSMC of this proposed scheme incorporates observer information, including the error differential signal and the estimated multisource disturbance information. This utilization of observer information allows the proposed scheme to avoid the inherent challenges associated with pure TSMC.

B. Stability Analysis of the Proposed Scheme

Substituting the first equation in (22) into (23) can yield

$$\hat{\sigma} = \hat{f}_e - b_0 I_s + h_1\left(e_m - \hat{e}_m\right) + c|e_m|^{\alpha} sat\left(e_m\right). \tag{25}$$

Substituting I_s in (24) into (25) can yield

$$\begin{aligned} \hat{\sigma} &= \hat{f}_e - b_0 I_{eq} - b_0 I_n - \hat{f}_e + h_1\left(e_m - \hat{e}_m\right) \\ &\quad + c|e_m|^{\alpha} sat\left(e_m\right) \\ &= h_1\left(e_m - \hat{e}_m\right) - b_0 I_n = -b_0 I_n. \end{aligned} \tag{26}$$

According to (24) and (26), the derivative of the sliding mode surface can be written as

$$\frac{d}{dt}\hat{\sigma} = -b_0 \frac{d}{dt} I_n = -k \mathrm{sgn}\left(\hat{\sigma}\right). \tag{27}$$

According to (27), the sliding mode condition (11) can be proven as follows:

$$\hat{\sigma}\frac{d}{dt}\hat{\sigma} = -\hat{\sigma} k \mathrm{sgn}\left(\hat{\sigma}\right) = -k\left|\hat{\sigma}\right|. \tag{28}$$

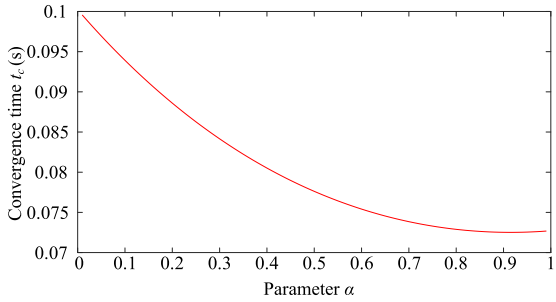

Fig. 4. Relationship between the convergence time t_c and the parameter α.

Once the condition $k > 0$ is satisfied, the speed error e_m can converge to zero in finite time.

C. Parameter Tuning of the Proposed Scheme

According to (22), (23), and (24), the proposed scheme contains 7 parameters, namely h_1, h_2, k_{r1}, k_{r2}, c, α, and k. The tuning methods of these parameters are presented as follows:

1) The tuning method of parameters h_1 and h_2: The h_1 and h_2 are the GI-EESO gains. According to [28], a bandwidth parametrization method is that

$$h_1 = 2\omega_o, \quad h_2 = \omega_o^2 \tag{29}$$

where ω_o is viewed as the bandwidth of the observer. It mainly affects the antidisturbance performance of the observer, which can be used as the performance index to set the value of ω_o. However, ω_o cannot be excessively large, as this can amplify the high-frequency noise in the speed loop, resulting in system instability. Thus, the selection of ω_o should be a tradeoff between the dynamic response performance and the system stability.

2) The tuning method of parameters k_{r1} and k_{r2}: The k_{r1} and k_{r2} are the gains of GIs. From [8] and [31], increasing the parameter k_r (k_{r1} and k_{r2}) can increase the GI gain near the resonant frequency. This means that the parameter k_r mainly affects the antidisturbance performance of the GI, which is used as the performance index to set the values of k_{r1} and k_{r2}.

3) The tuning method of parameter c: The parameter c is the control law gain of the TSMC. From (10), the parameter c affects the convergence time, which is used as the performance index to set the values of c. However, an excessively large parameter c may cause the undesired chattering problem. Thus, c should be set by balancing the convergence time and the chattering level.

4) The tuning method of parameter α: The α is the index of the absolute value of the error (e_m). According to (10), the parameter α mainly affects the convergence time. It is worth mentioning that formula (10) calculates the convergence time of the error along the sliding mode surface. However, from Fig. 2, as the error approaches zero, the error convergence trajectory no longer converges along the direction of the sliding mode surface. Thus, formula (10) cannot be used to calculate the time for the error to converge to zero. But we can use the formula (10) to estimate the time for the error to converge to a very small value, such as 0.3.

Fig. 4 shows the relationship between the convergence time t_c and the parameter α. The tuning parameters are set as follows:

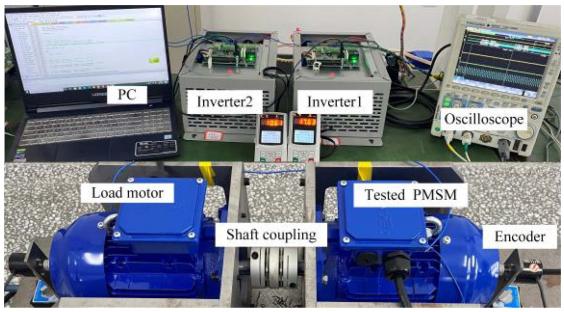

Fig. 5. Photograph of the PMSM experimental platform.

TABLE III
PARAMETERS OF THE TESTED PMSM

Quantity	Value	Quantity	Value
Rated power	2.2 kW	Number of pole pairs	3
Rated voltage	380 V	Stator resistance	1.025 Ω
Rated current	4.4 A	*D*-axis inductance	9 mH
Rated speed	3000 r/min	*Q*-axis inductance	18.5 mH
Rated torque	7 Nm	Flux linkage	0.249 Wb
Motor inertia	0.002379 kg·m^2		

$c = 50$, $e_m(0) = 5$, and $\Delta e_m = 0.5$. From Fig. 4, as the value of α increases, the convergence time t_c becomes shorter. Thus, the value of α should be set to a constant close to 1. Based on this, the parameter α is set to 0.9 in this article.

5) The tuning method of parameter k: The k is the switching gain of the TSMC. In pure TSMC, to ensure that it is robust to multisource disturbances, a large k is desired. However, this can lead to the undesired chattering problem. In the proposed scheme, since the multisource disturbances are suppressed by the GI-EESO, the parameter k can be set to a small value.

V. EXPERIMENTAL VERIFICATION

The proposed scheme has been experimentally assessed on a 2.2-kW PMSM platform, which is shown in Fig. 5. The parameters of the tested PMSM are listed in Table III. In this tested platform, a motor chip STM32F103 ARM serves as the control core. The PWM switching frequency is 6 kHz, and the PWM interrupt period is 166.7 μs to provide adequate execution time for the essential algorithms. For the experimental platform used, the current sampling error has a significant effect on the speed, while other disturbances have a minor effect. There are first and second speed harmonics caused by the current sampling error. In addition, the load torque is widely considered one of the most significant aperiodic disturbances in the speed loop. In this article, the proposed scheme is employed to suppress these disturbances to illustrate its effectiveness and feasibility.

To illustrate the advantages of the proposed scheme, in the following experiments, it is compared with the PI controller and pure TSMC, respectively. According to [6], the parameters of the PI controller are set as follows: $k_{sp} = 0.6$ and $k_{si} = 50.48$. The tuning parameters of pure TSMC are set as follows: $c = 18000$, $\alpha = 0.9$, and $k = 300$. According to Section IV-C, the parameters of the proposed scheme are set as follows: $c = 18000$, $\alpha = 0.9$, $k = 5$, $\omega_o = 750$, and $k_{r1} = k_2 = 10000$. In addition, the parameter b_0 is set to 235.49. It is worth mentioning that all these methods are implemented employing forward difference discretization [6], [32].

A. Limitation Verification of Pure TSMC

The antidisturbance performance of pure TSMC is verified under step load. According to [4] and [5], the multisource disturbances have the biggest impact on the system at medium and low speeds. Based on this, the speed is set to 200 r/min. Fig. 6 demonstrates the experimental results of pure TSMC with different k. With $k = 100$, it can be seen from Fig. 6(a) that the speed drop caused by the step load is 65 r/min, and the speed ripples are 16 r/min. From the Fourier analysis of the steady-state speed, there are mainly first and second speed harmonics. The first harmonic amplitude accounts for 0.67% of the base speed, and the second harmonic amplitude accounts for 1.82%. With $k = 300$, it can be seen from Fig. 6(b) that the speed drop caused by the step load is reduced to 52 r/min, and the speed ripples increase to 18 r/min. The first harmonic amplitude accounts for 0.65% of the base speed, and the second harmonic amplitude accounts for 0.75%. With $k = 500$, it can be seen from Fig. 6(c) that the speed drop caused by the step load is reduced to 42 r/min, and the speed ripples increase to 23 r/min. The first harmonic amplitude accounts for 0.59% of the base speed, and the second harmonic amplitude accounts for 0.55%. From the above analysis, the following two conclusions can be drawn.

1) The antidisturbance performance of pure TSMC is weak when the parameter k is small. Increasing parameter k can enhance the capability to suppress step load.
2) However, increasing k does not necessarily suppress periodic disturbances and may even cause more severe periodic disturbances. This is because increasing k will cause chattering in the controller output. From Fig. 6, increasing k will cause stator current (I_s) chattering, and this can also cause severe distortion of the phase current (i_a). The chattering of the stator current (I_s) can lead to speed ripples, deteriorating the steady-state performance of the output speed.

Therefore, pure TSMC is not suitable for suppressing multisource disturbances in the speed loop of PMSM drives.

B. Antidisturbance Performance Verification

To show the antidisturbance performance of the proposed scheme, it is compared with the traditional PI controller and pure TSMC, respectively. It is worth mentioning that to balance the antidisturbance performance and the chattering level, the switching gain k of pure TSMC is set to 300. Fig. 7 shows the comparative experimental results of the three different controllers under 100% rated load torque. With traditional PI controller, it can be seen from Fig. 7(a) that the speed drop caused by the step load is 99 r/min, and the speed ripples are 18 r/min. From the Fourier analysis of the steady-state speed, the first harmonic amplitude accounts for 2.54% of the base speed, the second harmonic amplitude accounts for 1.94%, and the total harmonic distortion (THD) is 3.24%. With pure TSMC, it can be seen from Fig. 7(b) that the speed drop caused by the step load is 52 r/min, and the speed ripples are 18 r/min. The first harmonic amplitude accounts for 0.65% of the base speed, the

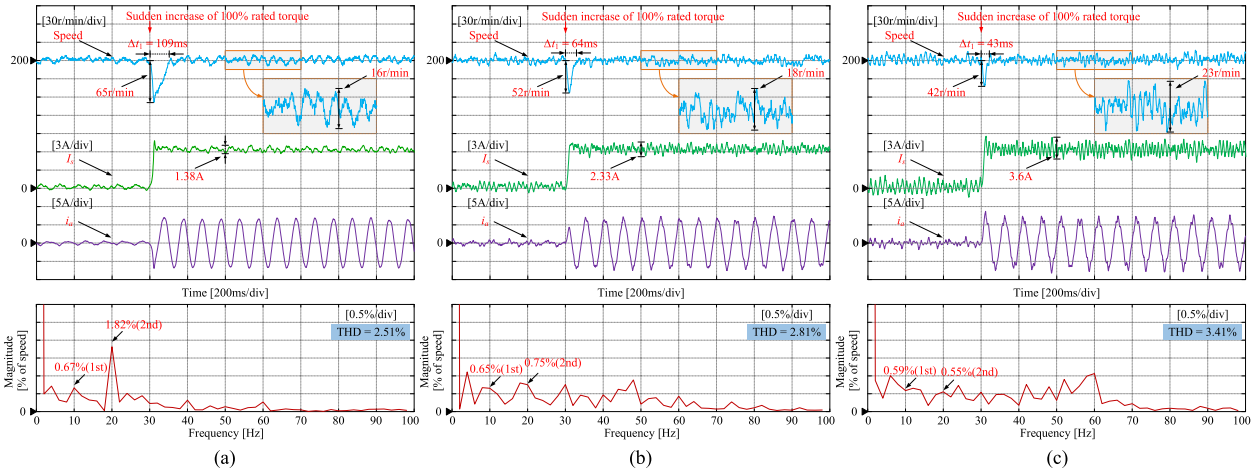

Fig. 6. Experimental results of pure TSMC with different k under 100% rated load torque. From top to bottom: speed, stator current, A-phase current, and Fourier analysis of steady-state speed. (a) $k = 100$. (b) $k = 300$. (c) $k = 500$.

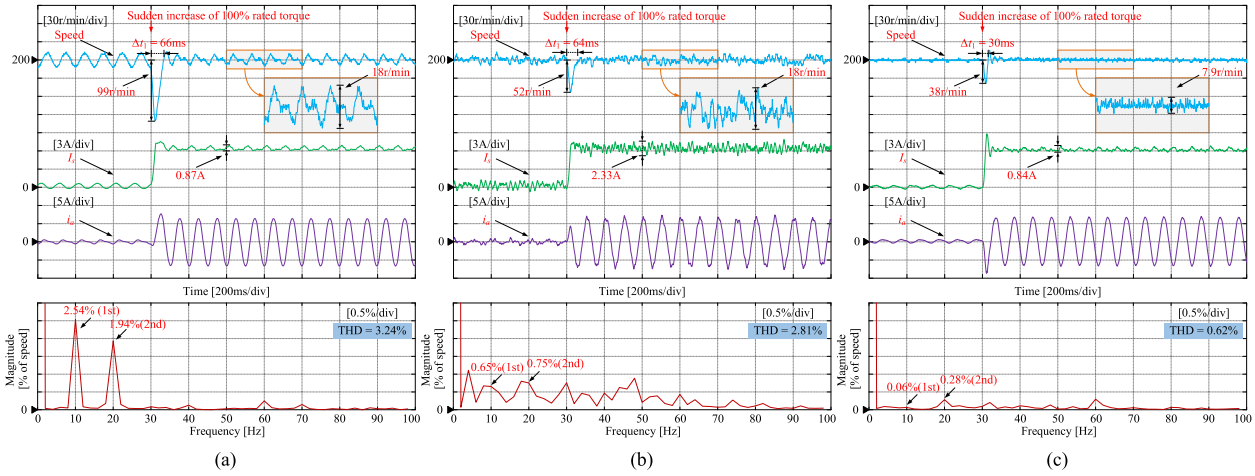

Fig. 7. Comparative experimental results of three different controllers under 100% rated load torque. From top to bottom: speed, stator current, A-phase current, and Fourier analysis of steady-state speed. (a) PI controller. (b) Pure TSMC ($k = 300$). (c) Proposed scheme.

second harmonic amplitude accounts for 0.75%, and the THD is 2.81%. With proposed scheme, it can be seen from Fig. 7(c) that the speed drop caused by the step load reduces to 38 r/min, and the speed ripples reduce to 7.9 r/min. The first harmonic amplitude accounts for 0.06% of the base speed, the second harmonic amplitude accounts for 0.28%, and the THD is 0.62%.

To clearly compare the antidisturbance performance of the three different control schemes, all the data related to the speed fluctuations are displayed in the radar diagram, as shown in Fig. 8. Two conclusions can be drawn from Fig. 8.

1) Compared with the PI controller, although pure TSMC can suppress the speed drop caused by step load, it cannot attenuate the speed ripples. Pure TSMC can suppress the first and second speed harmonics to a certain extent, but it can also introduce new speed harmonics due to the chattering problem. Overall, the speed ripples are not reduced in the speed loop.
2) Compared with pure TSMC, the proposed scheme can effectively suppress the multisource disturbances and reduce the speed drop and the speed ripples. The proposed scheme also eliminates the inherent chattering problem

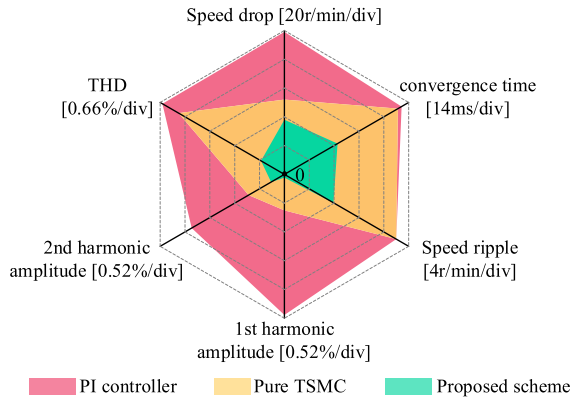

Fig. 8. Comparative radar diagram of antidisturbance performance of three different control schemes.

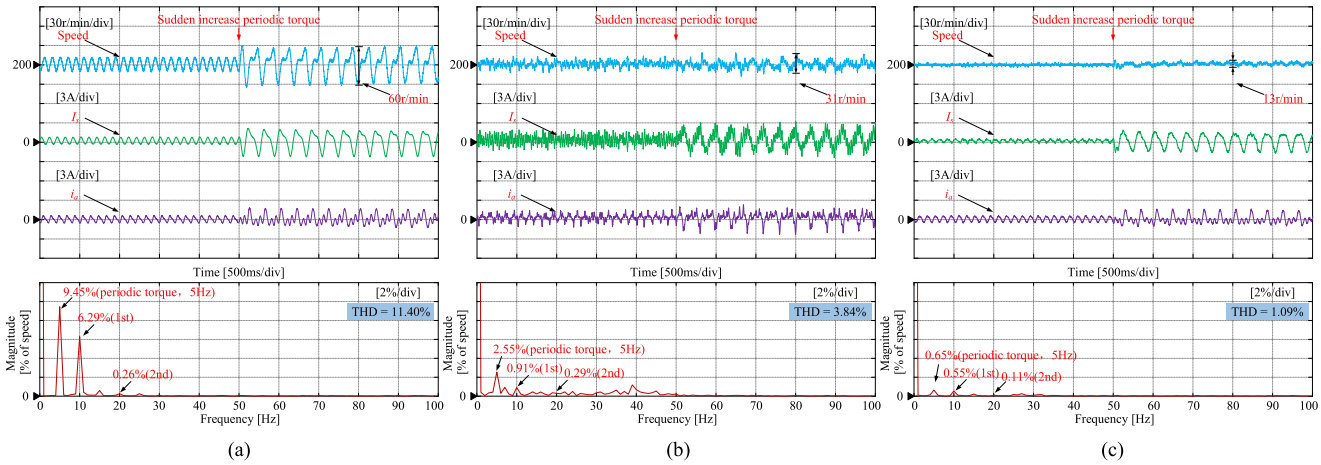

Fig. 9. Comparative experimental results of three different controllers under 20%-rated periodic load. From top to bottom: speed, stator current, A-phase current, and Fourier analysis of steady-state speed. (a) PI controller. (b) Pure TSMC ($k = 300$). (c) Proposed scheme.

of the TSMC. This is because the proposed scheme no longer relies on the large switching gain to suppress the disturbances in the speed loop. Instead, it suppresses the multisource disturbances through the introduced GI-EESO. Therefore, compared with pure TSMC, the proposed scheme is more suitable for suppressing multisource disturbances in the speed loop of PMSM drives.

C. Periodic Load Suppression Capability Verification

To evaluate the capability of the proposed scheme to suppress the periodic load, Fig. 9 shows the comparative experimental results of three different controllers under 20%-rated periodic load. With traditional PI controller, it can be seen from Fig. 9(a) that the speed ripples caused by the periodic disturbance are 60 r/min. From the Fourier analysis of the steady-state speed, it can be seen that the THD is 11.40%, and the speed harmonic caused by the periodic load accounts for 9.45% of the base speed. With pure TSMC, it can be seen from Fig. 9(b) that the speed ripples are 31 r/min. The THD is 3.84%, and the speed harmonic caused by the periodic load accounts for 2.55% of the base speed. With proposed scheme, it can be seen from Fig. 9(c) that the speed ripples are 13 r/min. The THD is 1.09%, and the speed harmonic caused by the periodic load accounts for 0.65% of the base speed. To sum up, compared with the traditional PI controller, pure TSMC can suppress the speed ripples caused by the periodic load to a certain extent, but it is difficult to completely suppress them. Different from this, the proposed scheme can effectively suppress the speed ripples caused by the periodic load and achieve smooth speed control.

D Parameter Robustness Verification

To evaluate the parameter robustness of the pure TSMC and the proposed scheme, verification was performed in the presence of parameter mismatch. According to (8), (12), (22), and (24), both pure TSMC and the proposed scheme are only related to the parameter b_0, which is the function of the rotor flux and the rotational inertia. Thus, b_0 is selected as the tested parameter, and its values are set to $0.5b_0$, $1.0b_0$, and $1.5b_0$, respectively. Fig. 10 shows the experimental results of the pure TSMC ($k = 300$) under parameter mismatch, while Fig. 11 shows the experimental results of the proposed scheme under parameter mismatch. From Figs. 10 and 11, both pure TSMC and the proposed scheme can still operate stably under parameter mismatch. Compared with pure TSMC, the proposed scheme is less affected by parameter mismatch. Therefore, the proposed scheme has good robustness to parameter mismatch.

E. Dynamic Response Performance Verification

To evaluate the dynamic response performance of the proposed scheme, experimental verification is conducted under speed-step change conditions. Fig. 12 shows the dynamic response experimental results of three different controllers. With traditional PI controller, it can be seen from Fig. 12(a) that there is an obvious speed overshoot. In addition, when the speed is 100 r/min or 200 r/min, the speed fluctuates seriously. With pure TSMC, it can be seen from Fig. 12(b) that there is no obvious speed overshoot. This indicates that pure TSMC has good dynamic response performance. However, when working under steady-state speed conditions, the speed fluctuates seriously, especially when the speed is zero. With the proposed scheme, it can be seen from Fig. 12(c) that there is a slight oscillation in the speed, which is caused by the GI in the proposed scheme. This mainly demonstrates the process of suppressing speed fluctuations through the proposed scheme. Compared with the PI controller and pure TSMC, the proposed scheme can not only suppress the speed fluctuations under different steady-state speed conditions, but also show superior dynamic response performance.

F. Verification Under Multiple Operating Conditions, Including On-Load Starting, Braking, and Reversal

Fig. 13 presents the experimental results of three different controllers in various modes under 100% rated load torque, including on-load starting, braking, and reversal. In Fig. 13,

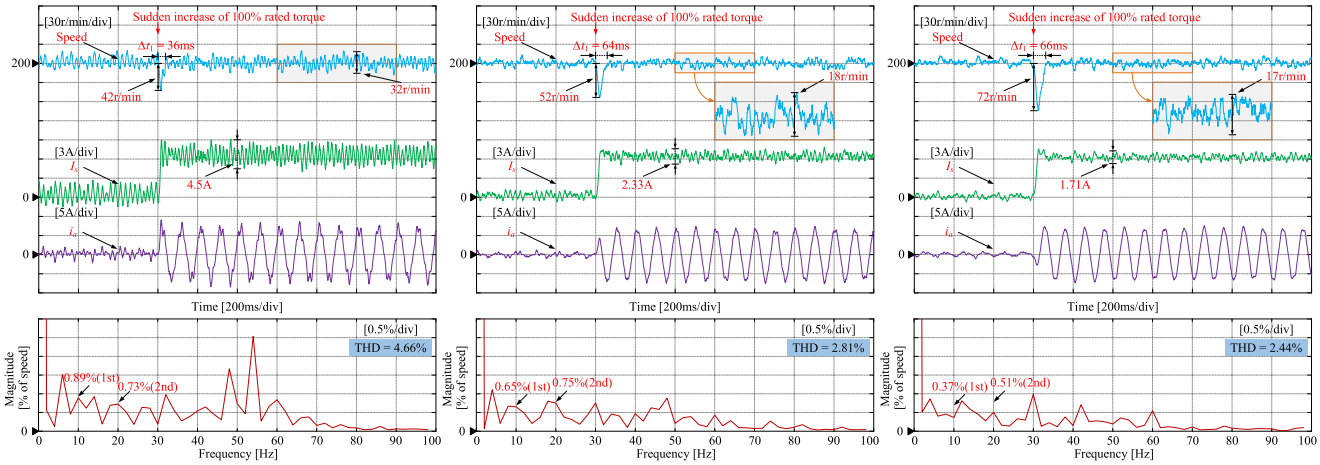

Fig. 10. Experimental results of pure TSMC ($k = 300$) under parameter mismatch. From top to bottom: speed, stator current, A-phase current, and Fourier analysis of steady-state speed. (a) $0.5b_0$. (b) 1.0 b_0. (c) $1.5b_0$.

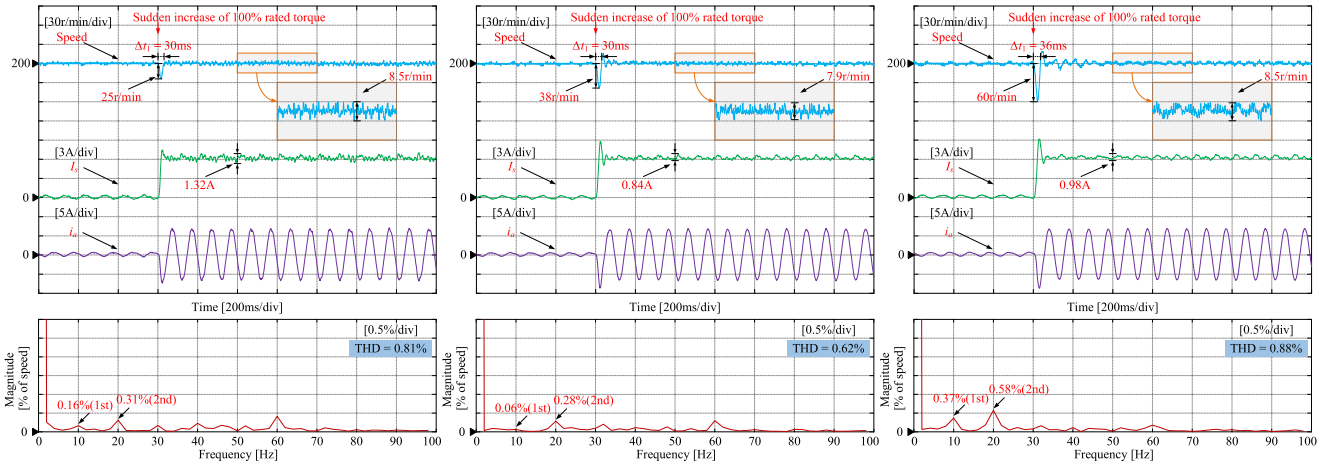

Fig. 11. Experimental results of the proposed scheme under parameter mismatch. From top to bottom: speed, stator current, A-phase current, and Fourier analysis of steady-state speed. (a) $0.5b_0$. (b) 1.0 b_0. (c) $1.5b_0$.

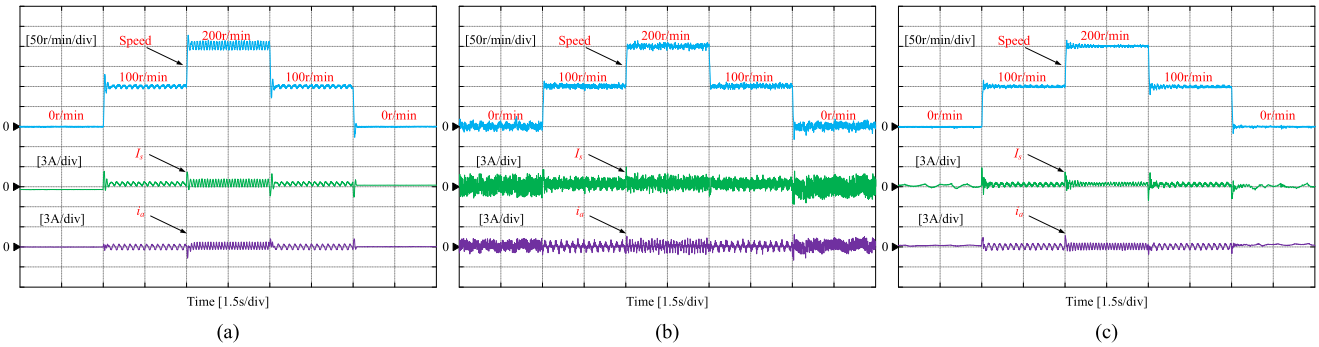

Fig. 12. Dynamic response experimental results of three different controllers. (a) PI controller. (b) Pure TSMC ($k = 300$). (c) Proposed scheme.

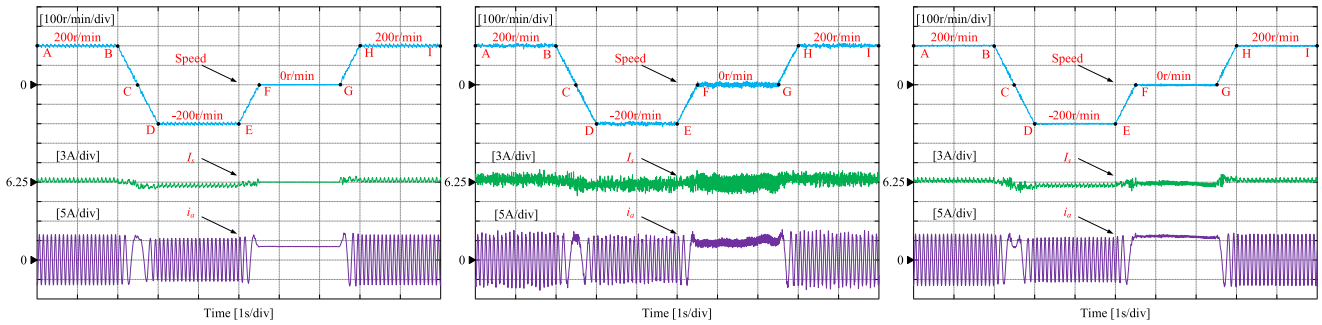

Fig. 13. Comparative experimental results of three different controllers in various modes under 100% rated load torque, including on-load starting, braking, and reversal. (a) PI controller. (b) Pure TSMC ($k = 300$). (c) Proposed scheme.

the experimental results of sections AB, DE, FG, and HI show the speed steady-state performance. The experimental results of segment BCD demonstrate the speed reversal performance. The experimental results of segment EF demonstrate the braking performance. In addition, the experimental results of segment FGHI show the performance of on-load starting. According to Fig. 13, three different control methods can always operate stably. Thus, employing the proposed scheme as the speed controller can ensure the stable operation of the motor in modes such as loaded start-up, braking, and reverse. Additionally, it is worth mentioning that, as can be seen from Fig. 13, the proposed scheme can effectively suppress speed ripples at different speeds and achieve high-precision speed control.

VI. Conclusion

In this article, an integrated observer-based TSMC was proposed to improve speed control accuracy by suppressing the multisource disturbances in the speed loop of PMSM drives. Compared with the existing TSMC, the proposed scheme has three significant advantages: First, it can further suppress the periodic disturbance. Second, it can avoid the differential calculation. Third, it is an integrated observer-based TSMC structure, and it is well compatible with industrial controllers. The proposed scheme has been verified on a 2.2-kW PMSM setup. The experimental results demonstrate that the proposed scheme can effectively suppress the multisource disturbances to enhance speed control accuracy. The results also show that the proposed scheme has good robustness to parameter mismatch. With the merits of the integrated structure and the antidisturbance capability against multisource disturbances, the proposed scheme can also be applied in the current loop or voltage loop of PMSM drives.

References

[1] J. Zhao, C. Yang, W. Gao, and L. Zhou, "Reinforcement learning and optimal control of PMSM speed servo system," *IEEE Trans. Ind. Electron.*, vol. 70, no. 8, pp. 8305–8313, Aug. 2023.

[2] J. Yang, J. Zhou, H. Zhou, F. Yi, D. Song, and M. Dong, "High-precision harmonic current extraction for PMSM based on multiple reference frames considering speed harmonics," *IEEE Trans. Ind. Electron.*, vol. 70, no. 10, pp. 9764–9776, Oct. 2023.

[3] J. Yang, W. Chen, S. Li, L. Guo, and Y. Yan, "Disturbance/uncertainty estimation and attenuation techniques in PMSM drives—A survey," *IEEE Trans. Ind. Electron.*, vol. 64, no. 4, pp. 3273–3285, Apr. 2017.

[4] Z. Zhou, C. Xia, Y. Yan, Z. Wang, and T. Shi, "Disturbances attenuation of permanent magnet synchronous motor drives using cascaded predictive -integral-resonant controllers," *IEEE Trans. Power Electron.*, vol. 33, no. 2, pp. 1514–1527, Feb. 2018.

[5] J. Liu, H. Li, and Y. Deng, "Torque ripple minimization of PMSM based on robust ILC via adaptive sliding mode control," *IEEE Trans. Power Electron.*, vol. 33, no. 4, pp. 3655–3671, Apr. 2018.

[6] L. Harnefors, S. E. Saarakkala, and M. Hinkkanen, "Speed control of electrical drives using classical control methods," *IEEE Trans. Ind. Appl.*, vol. 49, no. 2, pp. 889–898, Mar./Apr. 2013.

[7] Y. Yin et al., "Disturbance and uncertainty attenuation for speed regulation of PMSM servo system using adaptive optimal control strategy," *IEEE Trans. Transport. Electrific.*, vol. 9, no. 2, pp. 3410–3420, Jun. 2023.

[8] Y. Zuo et al., "Active disturbance rejection controller for smooth speed control of electric drives using adaptive generalized integrator extended state observer," *IEEE Trans. Power Electron.*, vol. 38, no. 4, pp. 4323–4334, Apr. 2023.

[9] Y. Wang, Y. Feng, X. Zhang, and J. Liang, "A new reaching law for antidisturbance sliding-mode control of PMSM speed regulation system," *IEEE Trans. Power Electron.*, vol. 35, no. 4, pp. 4117–4126, Apr. 2020.

[10] L. Zhang, Z. Chen, X. Yu, J. Yang, and S. Li, "Sliding-mode-based robust output regulation and its application in PMSM servo systems," *IEEE Trans. Ind. Electron.*, vol. 70, no. 2, pp. 1852–1860, Feb. 2023.

[11] C. Wang, F. Liu, J. Xu, and J. Pan, "An SMC-based accurate and robust load speed control method for elastic servo system," *IEEE Trans. Ind. Electron.*, vol. 71, no. 3, pp. 2300–2308, Mar. 2024.

[12] M. Muthusamy, J. Hendershot, and P. Pillay, "Design of a spoke type PMSM with SMC stator core for traction applications," *IEEE Trans. Ind. Appl.*, vol. 59, no. 2, pp. 1418–1436, Mar./Apr. 2023.

[13] X. Zhang, L. Sun, K. Zhao, and L. Sun, "Nonlinear speed control for PMSM system using sliding-mode control and disturbance compensation techniques," *IEEE Trans. Power Electron.*, vol. 28, no. 3, pp. 1358–1365, Mar. 2013.

[14] V. Q. Leu, H. H. Choi, and J.-W. Jung, "Fuzzy sliding mode speed controller for PM synchronous motors with a load torque observer," *IEEE Trans. Power Electron.*, vol. 27, no. 3, pp. 1530–1539, Mar. 2012.

[15] B. Wang, T. Wang, Y. Yu, and D. Xu, "Second-order terminal sliding-mode speed controller for induction motor drives with nonlinear control gain," *IEEE Trans. Ind. Electron.*, vol. 70, no. 11, pp. 10923–10934, Nov. 2023.

[16] W. Xu et al., "Improved adaptive terminal sliding-mode reaching law for speed control of TPMLSM with disturbance observer," *IEEE Trans. Ind. Appl.*, vol. 59, no. 3, pp. 3210–3219, May/Jun. 2023.

[17] D. Ginoya, P. D. Shendge, and S. B. Phadke, "Sliding mode control for mismatched uncertain systems using an extended disturbance observer," *IEEE Trans. Ind. Electron.*, vol. 61, no. 4, pp. 1983–1992, Apr. 2014.

[18] J. Yim, S. You, Y. Lee, and W. Kim, "Chattering attenuation disturbance observer for sliding mode control: Application to permanent magnet synchronous motors," *IEEE Trans. Ind. Electron.*, vol. 70, no. 5, pp. 5161–5170, May 2023.

[19] Z. Wang, S. Li, and Q. Li, "Discrete-time fast terminal sliding mode control design for DC–DC buck converters with mismatched disturbances," *IEEE Trans. Ind. Inform.*, vol. 16, no. 2, pp. 1204–1213, Feb. 2020.

[20] P. Kumar, D. V. Bhaskar, R. K. Behera, and U. R. Muduli, "Continuous fast terminal sliding surface-based sensorless speed control of PMBLDCM drive," *IEEE Trans. Ind. Electron.*, vol. 70, no. 10, pp. 9786–9798, Oct. 2023.
[21] K. Shao, J. Zheng, K. Huang, H. Wang, Z. Man, and M. Fu, "Finite-time control of a linear motor positioner using adaptive recursive terminal sliding mode," *IEEE Trans. Ind. Electron.*, vol. 67, no. 8, pp. 6659–6668, Aug. 2020.
[22] B. Xu, L. Zhang, and W. Ji, "Improved non-singular fast terminal sliding mode control with disturbance observer for PMSM drives," *IEEE Trans. Transport. Electrific.*, vol. 7, no. 4, pp. 2753–2762, Dec. 2021.
[23] K. Zhang, L. Wang, and X. Fang, "High-order fast nonsingular terminal sliding mode control of permanent magnet linear motor based on double disturbance observer," *IEEE Trans. Ind. Appl.*, vol. 58, no. 3, pp. 3696–3705, May/Jun. 2022.
[24] W. Xu, A. K. Junejo, Y. Liu, and M. R. Islam, "Improved continuous fast terminal sliding mode control with extended state observer for speed regulation of PMSM drive system," *IEEE Trans. Veh. Technol.*, vol. 68, no. 11, pp. 10465–10476, Nov. 2019.
[25] S. Li, M. Zhou, and X. Yu, "Design and implementation of terminal sliding mode control method for PMSM speed regulation system," *IEEE Trans. Ind. Inform.*, vol. 9, no. 4, pp. 1879–1891, Nov. 2013.
[26] T. Shi, Z. Wang, and C. Xia, "Speed measurement error suppression for PMSM control system using self-adaption Kalman observer," *IEEE Trans. Ind. Electron.*, vol. 62, no. 5, pp. 2753–2763, May 2015.
[27] K. Ogata *Modern Control Engineering*, 3rd ed. Hoboken, NJ, USA: Prentice-Hall, 1996.
[28] Z. Gao, "Scaling and bandwidth-parameterization based controller tuning," in *Proc. Amer. Control Conf.*, 2003, pp. 4989–4996.
[29] W.-H. Chen, J. Yang, L. Guo, and S. Li, "Disturbance-observer-based control and related methods—An overview," *IEEE Trans. Ind. Electron.*, vol. 63, no. 2, pp. 1083–1095, Feb. 2016.
[30] R. Madonski, S. Shao, H. Zhang, Z. Gao, J. Yang, and S. Li, "General error-based active disturbance rejection control for swift industrial implementations," *Control Eng. Pract.*, vol. 84, pp. 218–229, 2019.
[31] B. Guo, S. Bacha, M. Alamir, A. Hably, and C. Boudinet, "Generalized integrator-extended state observer with applications to grid-connected converters in the presence of disturbances," *IEEE Trans. Control Syst. Technol.*, vol. 29, no. 2, pp. 744–755, Mar. 2021.
[32] K. Ogata, *Discrete-Time Control Systems*. Hoboken, NJ, USA: Prentice-Hall, 1995.

Minghe Tian was born in Henan Province, China, in 1996. He received the B.S. degree from Northeastern University, Shenyang, China, in 2018, and the M.S. degree from Harbin Institute of Technology, Harbin, China, in 2020, both in electrical engineering, where he is currently working toward the Ph.D. degree in electrical engineering.

His research interests include permanent magnet synchronous motor drives and antidisturbance control theory.

Tianqing Wang was born in Heilongjiang Province, China, in 1997. He received the B.S. and M.S. degrees in electrical engineering in 2019 and 2021, respectively, from Harbin Institute of Technology, Harbin, China, where he is currently working toward Ph.D. degree in power electronics and electrical drives with the School of Electrical Engineering and Automation.

His research interests include sliding-mode control and sensorless induction motor drives.

Yong Yu was born in Jilin Province, China, in 1974. He received the B.S. degree in electromagnetic measurement and instrumentation, and the M.S. and Ph.D. degrees in electrical engineering from Harbin Institute of Technology (HIT), Harbin, China, in 1995, 1997, and 2003, respectively.

From 2004 to 2014, he was an Associate Professor with the Department of Electrical Engineering, HIT, where he has been a Professor of Electrical Engineering since 2014. His current research interests include ac motor drives, power quality mitigation, and fault diagnosis and tolerant control of inverter.

Qinghua Dong was born in Shandong Province, China, in 1994. He received the B.S. degree in electrical engineering from China University of Mining and Technology, Xuzhou, China, in 2016, and the M.S. degree in electrical engineering in 2018 from Harbin Institute of Technology, Harbin, China, where he is currently working toward the Ph.D. degree in electrical engineering.

His research interests include ac motor drives and model predictive control.

Bo Wang (Member, IEEE) was born in Shandong Province, China, in 1987. He received the B.S. degree from Northwestern Polytechnical University, Xi'an, China, in 2011, and the M.S. and Ph.D. degrees from Harbin Institute of Technology (HIT), Harbin, China, in 2013 and 2017, respectively, all in electrical engineering.

In 2017, he was with the School of Electrical Engineering and Automation, HIT, where he is currently an Associate Professor of electrical engineering. He has authored more than 50 technical papers published in journals and conference proceedings. His research interests include ac motor drive, ac servo drive system, position-sensorless control, and nonlinear control theory.

Dianguo Xu (Fellow, IEEE) received the B.S. degree in control engineering from Harbin Engineering University, Harbin, China, in 1982, and the M.S. and Ph.D. degrees in electrical engineering from Harbin Institute of Technology (HIT), Harbin, China, in 1984 and 1989, respectively.

In 1984, he was with the Department of Electrical Engineering, HIT as an Assistant Professor. Since 1994, he has been a Professor with the Department of Electrical Engineering, HIT. He was the Dean with the School of Electrical Engineering and Automation, HIT, from 2000 to 2010. He was the Vice President of HIT from 2014 to 2020. He has authored and coauthored more than 600 technical papers. His research interests include renewable energy generation technology, power quality mitigation, sensorless vector-controlled motor drives, and high performance PMSM servo system.

Dr. Xu is the Co-EIC of IEEE TRANSACTIONS ON POWER ELECTRONICS and the Associate Editor for IEEE TRANSACTIONS ON INDUSTRIAL ELECTRONICS. He is a Chairman of IEEE Harbin Section.